

# Revisiting Point Cloud Completion: Are We Ready For The Real-World?

Stuti Pathak  
University of Antwerp

stuti.pathak@uantwerpen.be

Prashant Kumar  
Indian Institute of Technology Delhi

prashantk.nan@gmail.com

Nicholus Mboga  
University of Antwerp

nicholus.mboga@gim.be

Gunther Steenackers  
University of Antwerp  
gunther.steenackers@uantwerpen.be

Rudi Penne  
University of Antwerp  
rudi.penne@uantwerpen.be

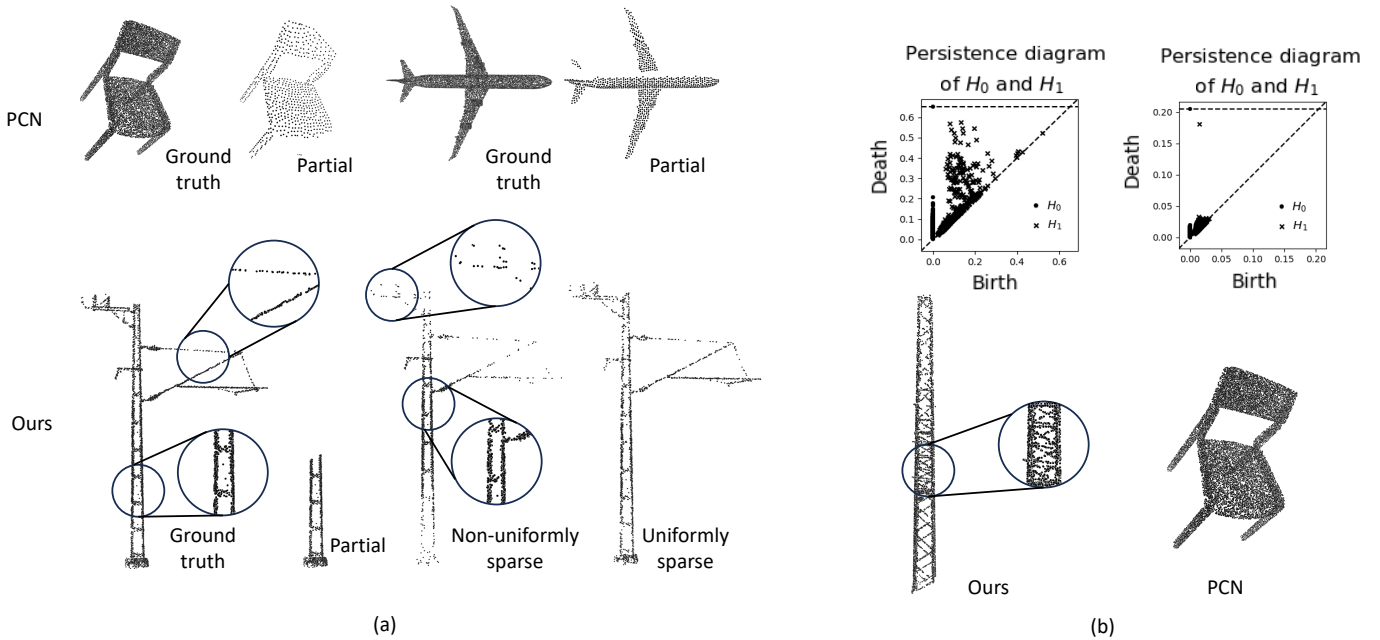


Figure 1: Qualitative comparison of synthetic and real-world object point clouds. (a) We show a complete absence of non-uniformity and noise for the synthetic PCN dataset, in contrast to multiple-levels of non-uniformity (as shown by the magnified regions) along with noise (bottom two magnifications) in the case of our **RealPC** dataset. (b) Comparison of Persistence Diagrams of a point cloud from **RealPC** vs PCN dataset. Points further away from the diagonal indicate strong topological features. **RealPC** has numerous significant 0 and 1-dimensional ( $H_0, H_1$ ) topological features.

## Abstract

Point clouds acquired in constrained and challenging real-world settings are incomplete, non-uniformly sparse, or both. These obstacles present acute challenges for a vital task - point cloud completion. Using tools from Algebraic Topology and Persistent Homology ( $\mathcal{PH}$ ), we demonstrate that current benchmark synthetic point clouds lack rich

topological features that are important constituents of point clouds captured in realistic settings. To facilitate research in this direction, we contribute the first real-world industrial point cloud dataset for point cloud completion, **RealPC** - a diverse set of rich and varied point clouds, consisting of  $\sim 40,000$  pairs across 21 categories of industrial structures in railway establishments. Our benchmark results on several strong baselines reveal a striking observation - the existing

methods are tailored for synthetic datasets and fail miserably in real-world settings. Building on our observation that **RealPC** consists of several 0 and 1-dimensional  $\mathcal{PH}$ -based topological features, we demonstrate the potential of integrating Homology-based topological priors into existing works. More specifically, we present how 0-dimensional  $\mathcal{PH}$  priors, which extract the global topology of a complete shape in the form of a 3-D skeleton, can assist a model in generating topologically-consistent complete shapes.

## 1 Introduction

In its simplest form, a point cloud is a discrete surface-sampling of an object or an environment, which can be further processed to generate corresponding 3D models. With the growing interest in generating such digital twins of our real-world over the years, point clouds can now be obtained using various sensors and techniques, such as LiDAR, depth cameras, photogrammetry, structured light scanning, etc. Their ability to represent complex shapes with attention to local intricate details makes them indispensable across numerous fields, such as robotics [26], autonomous driving [58], medical image analysis [62], augmented and virtual reality [35], remote sensing and geoinformatics [28], etc.

Inherently, real-world point clouds are non-uniformly sparse and have rich topological features, unlike synthetic point clouds (Figure 1). They may have missing parts due to occlusions, view angle constraints, light reflectivity and object surface properties, multiple resolutions when more than one type of sensor is used, environmental factors such as fog and dust, etc. This hinders the performance of all downstream point cloud tasks, for instance, registration, surface reconstruction, object recognition, segmentation, etc. As a result, obtaining the full 3D shape representation from an incomplete and sparse point cloud plays a vital role in the practical applications of point cloud datasets. With the rise of data-driven methods, this area has been widely investigated under the umbrella term *point cloud completion* [21, 64, 45].

Although historically motivated from a real-world perspective, as discussed above, most of the existing models in the field of machine learning-based point cloud completion report their performances on mostly synthetic datasets [48, 61, 13, 31, 52, 63]. This stems from the easy accessibility, simpler shapes, minimal to no noise, and uniformly-distributed points typically found in synthetically-generated point cloud datasets such as PCN [59], Completion3D [43], ShapeNet55/34 [56], MVP [36]. However, due to the excessive tailoring of these models to such synthetic datasets, they fall short of providing similar results for realistic datasets, as we will see in the upcoming sections.

The unordered representation of a point cloud does not

allow for the encoding of any structural information. This makes point cloud processing very challenging. Persistent Homology has been shown to learn global structural properties of datasets. It is a powerful tool from topological data analysis (TDA) that has gained traction in 3D vision applications, particularly for analyzing and understanding the underlying shape and structure of data from different modalities - point clouds, images, graphs, [42, 34, 8] etc. It helps in identifying topological features, such as connected components, loops, and voids, across multiple scales. However, as far as our knowledge goes this line of research has not yet been explored for the task of completing point clouds in general, let alone real-world ones.

## 2 Related Work

### 2.1 Benchmark Object-Level Point Cloud Datasets

Not only is the processing of real-world point cloud data arduous but also its acquisition comes with its own set of challenges. With the availability of high-end 3D-scanning devices nowadays, this task ultimately boils down to balancing the time involved, the accuracy required, and the setup costs. In addition, there is no particular standard storage format followed by the available sensors in the market today. Moreover, such point cloud datasets have background outliers which can make most of the modern data-driven algorithms blow up and therefore demand manual outlier removal, which is extremely time-consuming. All of these factors combined pose a great difficulty in accessing and working with realistic point cloud data and introduce an inevitable hurdle for 3D vision research community. Hence, researchers prefer working on synthetically generated datasets instead. We now provide a brief discussion on all existing benchmark datasets on which recent SoTA point cloud completion models have experimented on.

The PCN dataset [59] contains paired partial and complete point clouds derived from 30,974 CAD models across 8 categories from the ShapeNet repository [11]. Two more datasets derived from the same CAD repository [11] are ShapeNet55 and ShapeNet34 datasets [56]. ShapeNet-55 includes 52,470 objects from 55 categories. The ShapeNet-34 dataset is derived by splitting the original ShapeNet-55 dataset into 34 seen categories and 21 unseen categories. Another synthetic dataset is the MVP dataset [36], which consists of more than 100,000 point clouds from 16 categories sampled again from CAD models.

Although fewer in number, some recent real-world point cloud object datasets include OmniObject3D [51], MatterPort3D [10], ScanNet [17], and KITTI [25]. The ScanNet and MatterPort3D datasets offer 3D reconstructions of in-

door spaces, while the KITTI dataset captures scenes from outdoor environments. All of these datasets are unpaired and hence contain only partial shapes and no ground truth, naturally making them infeasible for supervised training.

## 2.2 Point Cloud Completion

Point cloud completion has been extensively studied on synthetic point clouds (e.g. PCN, Shapenet, etc). Most works approach this as a point features learning and per point generation problem. Voxel-based and point-based approaches have been primarily used for this task. GRNet [54] utilizes 3D CNNs and multilayer perceptrons (MLPs) for point cloud representation. However, voxel-based methods struggle with limited input points, resulting in incomplete voxel neighborhoods and hole-ridden outputs. This robustness limitation hinders their effectiveness. Point-based methods directly operate on the raw points. Started with PCN [59], several works [52, 50, 63] have used this strategy for effective completion. ODGNet [6] utilizes a Seed Generation U-Net for enhanced seed point representation. It incorporates Orthogonal Dictionaries to learn shape priors, compensating for missing information during inference. PointAttN [49] leveraging cross-attention and self-attention mechanisms, incorporating Geometric Details Perception (GDP) and Self-Feature Augment (SFA) blocks to establish structural relationships among points. PointTr [57] represents point clouds as unordered groups with position embeddings, converting them to point proxy sequences for generation via a transformer encoder-decoder architecture. There have been several such works [41, 60, 44, 37, 53, 50, 46, 30, 3, 55, 2] most of which revolve around the point feature learning-based encoder-decoder architecture. The current literature works well on synthetic point clouds, but their performance on real-world point clouds needs to be probed. We follow this line of work and demonstrate some interesting and contrasting observations in this direction.

## 2.3 Persistent Homology and Topological Deep Learning

Persistent Homology ( $\mathcal{PH}$ ) has its origins in algebraic topology and enables the measurement of topological features which characterize the shape of the data. Persistent Homology can be seen as an adaption of homology [20, 38, 5] in case of point clouds. It captures the evolutions of topological features (cycles, voids, etc.) in several dimensions (0, 1, 2) in a dataset.  $\mathcal{PH}$  is concreted with the study of invariants across multiple scales. Characterizing these features allows  $\mathcal{PH}$  to discern essential structures and patterns that is not possible using conventional methods. Topological methods have been recently used across several learning-based tasks. Several works

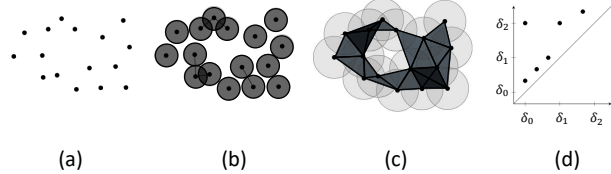


Figure 2: Left to Right (a to c). Progression of filtration on a point cloud over different spatial resolutions as the distance threshold increases [33]. Creation and destruction of  $k - dim$  topological features documented in (d) which is a persistence diagram representing  $(b_i, d_i)$  pairs - each point corresponds to a  $k - dim$  homology that takes birth at  $b_i$  and dies at  $d_i$ .

[27, 39, 29, 14, 32, 12, 18] have used topological tools to augment learning with better feature descriptors. Vectorized topological descriptors extracted using  $\mathcal{PH}$  have been used for interpretability of models [22], adversarial learning. [24] introduce topological representation for auto-encoding and demonstrate the topological richness of the learned representations.  $\mathcal{PH}$  has also been used for several geometric problems like - surface reconstruction, pose matching [9, 4, 18] etc. Several works have also proposed general-purpose differentiable topology layers to extract descriptors for topological regularization [23].

## 3 Background

A  $k$ -simplex is the convex hull of  $k + 1$  affinely independent points, forming a line (in 1D), triangle (in 2D), or a tetrahedron (in 3D), etc. A simplicial complex is a collection of simplices with simplex intersections. In topology, homology counts  $k$ -dimensional holes (0-D: connected components, 1-D: loops 2-D: voids), etc.

**Persistent Homology** -  $\mathcal{PH}$  is an algebraic method to discover topological features of datasets [20, 38, 5]. It converts a dataset (here, a point cloud) to a simplicial complex and studies the change of homology across a filtration sequence  $\phi \subseteq \mathcal{C}_1 \subseteq \mathcal{C}_2 \subseteq \mathcal{C}_3 \dots \mathcal{C}_i \dots \mathcal{C}_n = \mathcal{C}$ . A filtration is defined on edges of the complex using a filtration function  $f((v_0, v_1 \dots v_n)) = \max_{i < j; i, j \in \{0, 1, 2, 3 \dots n\}} f(v_i, v_j)$ . It is based on pairwise distance between points, and is monotonic, with each subsequent complex having a higher value. The evolution of Homology across a filtration sequence parameterized by  $\alpha$  is described here- Consider a set of points in 3D space - a point cloud. Filtration can be generated by increasing the radius of  $\alpha$ -neighborhood balls around each point (Table 9). Two points are connected by an edge when their balls intersect, i.e., distance  $\leq 2\alpha$ . The filtration progression as  $\alpha$  increase can be described as follows - For a given value of  $\alpha$ , we connect all points that

are within a distance of  $2\alpha$  from each other. As we increase  $\alpha$ , we introduce more and more edges, following a specific order. When an edge is added, it can potentially create higher-dimensional simplices, such as triangles or tetrahedrons. These simplices, along with the edges, are included in the filtration, with lower-dimensional simplices being added before higher-dimensional ones. As the filtration progresses, we observe the creation and destruction of topological features, known as homology. These features represent holes of different dimensions, such as connected components, cycles, and voids. The birth and death of these features are governed by the following principles - **(a)** Birth of a Feature: When an edge is added, it may create a new hole that was not present before. This marks the birth of a feature. **(b)**: Death of a Feature: When an edge is added, it may fill an existing hole completely. This leads to the death of the feature that was born when the hole first appeared. For instance, consider four points forming a rectangle. This creates a 1-dimensional hole (a cycle). When the diagonal edge is added later, it fills the rectangle with two triangles, causing the 1-dimensional hole to disappear. Each 1-dimensional hole has a specific birth value of  $\alpha$  and a death value of  $\alpha$ . The addition of an edge always results in either the creation or destruction of a homology. In the case of a point cloud or an image, we don't know the optimal values of  $\alpha$  to extract significant features. Therefore, we consider all possible values of  $\alpha$  and track the changes in homology. This creates a nested sequence of simplicial complexes, known as a filtration. Each hole has a birth-death pair  $(b, d)$ , representing its persistence. These pairs can be represented as points in the 2D graph where the diagonal  $(b = d)$  represents trivial pairs while points above the diagonal represent topological descriptors.

## 4 Object-Level Training Dataset Creation

In light of the challenges outlined in Section 2.1 concerning the acquisition of real-world point cloud datasets, in this section we demonstrate a methodology (Figure 4) to extract and process paired object point cloud datasets from existing open-source scene-level datasets. Their paired nature ensures suitability for any supervised point cloud completion algorithm, therefore, lowering the threshold for experimenting on real-world data. Although we have explored this methodology in a railway-environment setup, this exact procedure can be followed for any scene-level point cloud dataset.

We use four open-source railway datasets: [15] by Hungarian State Railways acquired with a Riegl VMX-450 high-density mobile mapping system; [40] by Wuhan University, in which urban railway dataset was captured using Optech's Lynx Mobile Mapper System, rural railway dataset with MLS system equipped with HiScan-Z LiDAR

sensors, and plateau railway dataset with Rail Mobile Measurement System (rMMS) equipped with a 32-line LiDAR sensor; [1] by SNCF Réseau, the French state-owned railway company; and a Catenary arch dataset [47] given by Strukton Rail, captured using Trimble TX8 Terrestrial Laser Scanner (TLS). A few scenes from these datasets have been visualized in Figure 3.

The mentioned scene-level point clouds are pre-annotated into relevant sections such as vegetation, overhead cables, railway tracks, industrial support and transmission structures, ground, etc. For this work, we extract industrial structures from these scene-level point clouds. As a result, we obtain a point cloud with multiple industrial structures as shown in Figure 4 Input to (A). Referring to the same figure, our methodology is divided into five main parts. In (A) we employ HDBSCAN [7], a hierarchical clustering algorithm, to cluster individual industrial structures. HDBSCAN works accurately for noisy and complex data and automatically detects the number of data clusters. In (B), a manual inspection is performed to extract industrial structures which can serve as good ground truth for supervised training. Finally, in (C), (D), and (E), we process these ground truth point clouds in three different ways to induce uniform sparsity, non-uniform sparsity, and incompleteness as explained in detail ahead.

For making a partial point cloud (C), we pick a random viewpoint around a ground truth point cloud and remove  $N$  number of points that are farthest away from this viewpoint. Similarly for sparsifying the same point cloud non-uniformly (D), we again pick a random viewpoint but this time we assign a probability to each point, which is either proportional or inversely proportional to a point's cubed distance to this viewpoint. Then, we sample  $N$  points based on these probability values. This is repeated for different values of  $N$  and for different viewpoints. For uniform sparsification (E), we randomly sample  $N$  points and then repeat for different values of  $N$ . Simultaneous to these steps, we perform manual noise-removal. These three steps are conducted for all ground truth point clouds to obtain a paired object-level training dataset.

As a final step, we manually examine all the industrial structures and classify them into 21 classes based on their geometric shapes. From now on we will call this dataset **RealPC**. On publication, to help advancement in this line of research, we will make this processed object-level training dataset as well as the code for this processing pipeline open-source.

### 4.1 Comparative Analysis

In this section, we conduct a comprehensive geometric and topological analysis and comparison of our dataset with PCN and ShapeNet-55/34 both qualitatively and quantita-

	Noise				Non-Uniformity				PH-based ( $H_0; H_1$ )			
	Class 1	Class 2	Class 3	Class 4	Class 1	Class 2	Class 3	Class 4	Class 1	Class 2	Class 3	Class 4
PCN	10.6	8.8	8.6	14.0	18.1	12.0	14.7	20.4	79.5; 34.2	52.4; 22.2	66.0; 31.9	87.1; 36.9
ShapeNet	9.8	12.2	14.9	11.2	13.9	14.6	20.2	17.8	44.4; 18.6	47.2; 20.2	66.0; 29.4	56.4; 26.5
<b>RealPC</b>	<b>137.4</b>	<b>99.2</b>	<b>93.1</b>	<b>92.5</b>	<b>234.2</b>	<b>222.4</b>	<b>128.1</b>	<b>148.2</b>	<b>382.3; 155.7</b>	<b>322.5; 114.9</b>	<b>341.2; 149.5</b>	<b>274.8; 126.4</b>

Table 1: Quantitative comparative analysis of **RealPC** against PCN and ShapeNet using three metrics - sum of 0 and 1-dimensional persistence of topological features, non-uniformity, and noise. Best values are bold-faced. All values are in units of  $10^{-4}$ . All numbers demonstrate that **RealPC** has stronger Homology-based topological features, non-uniformity and noise. For a visual demo see Fig. 1

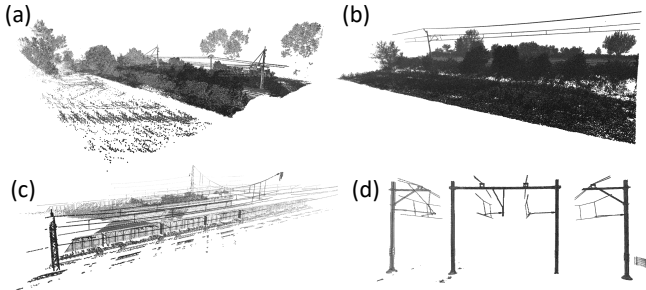


Figure 3: Scene-level point clouds from different acquisition techniques (a) [1], (b) [15], (c) [40], and (d) [47]

tively based on the following three factors:

- **Non-Uniformity:** For a point cloud we calculate the distance of all of its  $N$  points with their nearest neighbor and then find the standard deviation of all these distances across the entire point cloud. We report the average of all these standard deviation values across different classes of different datasets as *Non-Uniformity*.
- **Noise:** For each point in a point cloud we first fit a plane using linear regression over its  $k$ -nearest neighbors. Then we calculate the perpendicular distance from the said point to the said plane. We average this distance for all the points in our point cloud. Finally, we calculate the average of these average values, termed *Noise*, across different classes of different datasets.
- **Persistent Homology ( $H_0; H_1$ ):** Persistence Diagrams in  $\mathcal{PH}$  represent the (*birth, death*) of topological features across a filtration, as points on the  $x$ - $y$  plane. All points are above the diagonal ( $x = y$ ). Points further away from the diagonal represent features with a larger persistence ( $(death - birth)$ ), and hence are the most important topological features. We compute the average of  $death - birth$  averages for 0 & 1-*dim* topological features separately across all classes of all datasets and report them as *PH-based ( $H_0; H_1$ )*.

We pick four classes at random from PCN and ShapeNet datasets. Whereas, we divide our **RealPC** into four classes based on their sources. As presented in Table 1, our dataset shows the highest *Noise*, *Non-uniformity*, and *PH-based ( $H_0; H_1$ )* values consistently when compared to any of the other synthetic classes. This result is supported by the visualizations shown in Figure 1 (a) and (b). We can clearly see high non-uniformity and noise in point clouds from our dataset, in contrast to the complete absence of them in PCN. The (b) part of this figure investigates the existence of topological features in real and synthetic point clouds. The contrast between the two is striking. While persistence diagram for ours consists of numerous important 0 & 1-*dim* topological features, synthetic datasets (e.g. PCN) lack them. This is indicated by the presence of several points further from the diagonal for our dataset and their absence in PCN.

## 5 Experiments

Point Cloud completion is one of the fundamental tasks in point clouds perception-based challenges. In this section, we demonstrate the challenges in real-world point completion by benchmarking **RealPC** against several strong baselines. In order to gauge the maturity of the point cloud completion literature we benchmark them against several recent, strong, and relevant baselines that have shown remarkable performance on existing simulated datasets. We demonstrate that current state-of-the-art models are not adept at handling point clouds collected in real-world environments that have several contrasting characteristics from real-world point clouds. We demonstrate the performance of these models in Table 2.

### 5.1 Benchmarking

We benchmark baselines that have shown remarkable performance on existing datasets (ShapeNet, PCN, ShapeNet33, ShapeNet55). We use the following works and show their performance on **RealPC**: (a) ODGNet [6] (b) PointAttN [49] (c) SnowFlakeNet [52] (d) PointTr [57] (e) AdaPoinTr [57] (f) PartialToComplete [16] (g) TopNet [44]

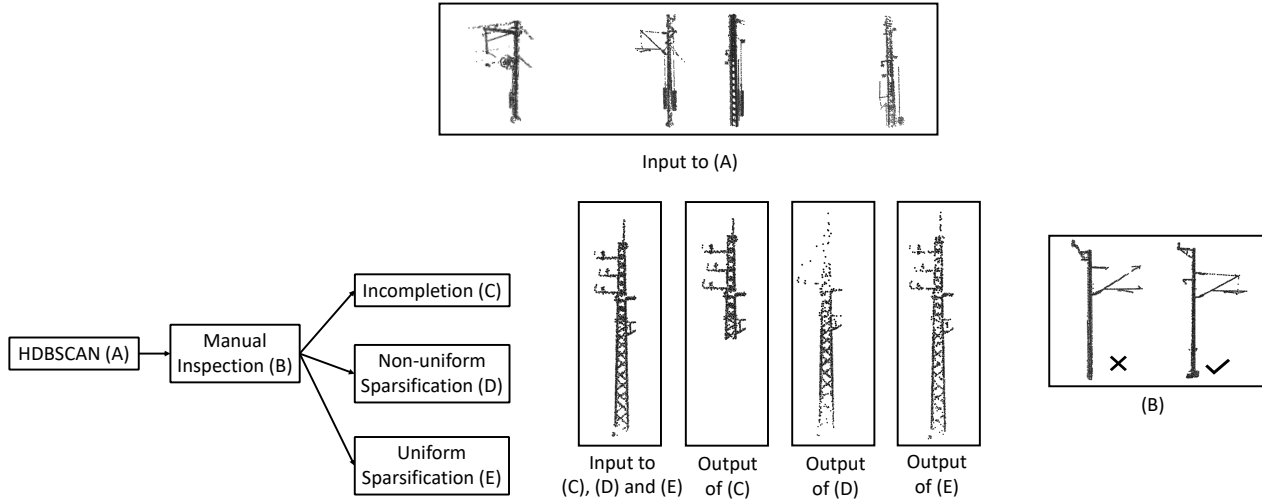


Figure 4: Object-level training dataset creation methodology. Input to (A) are the segmented industrial structures from scene-level point clouds. Figure (B) shows how manual inspection was done to extract ground truth data. Output of (C), (D), and (E) are the 3 variants of sparse and incomplete point clouds

(h) GrNet [54] (h) SeedFormer[63]. We use Chamfer Distance (L1) as a metric to measure the conformity of the completed shapes against the ground truth complete shapes.

## 5.2 Results

We now demonstrate the results of our benchmarking exercise in Table 2 and Figure 5. We demonstrate the completion performance of all the available baselines on **RealPC** across the available 21 classes. The results across all models demonstrate the challenges presented by **RealPC**. The benchmarked models fail miserably while generating complete shapes of partial incomplete point clouds from the **RealPC** dataset. These results demonstrate the gap between performance on real-world point clouds and current simulated point clouds that have been used in the literature.

## 5.3 Analysis

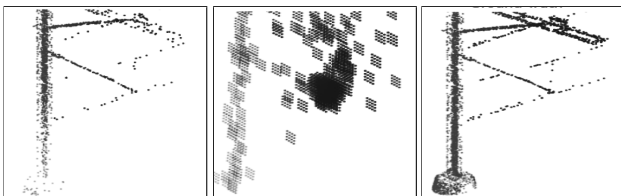


Figure 5: **Left**: Non-uniform sparse partial input to the best benchmarked baseline. **Middle**: Sub-optimal completion results. **Right**: Ground Truth complete point cloud.

We discuss the performance of the benchmarked baseline models on **RealPC** dataset. As demonstrated in Table 2 and Figure 5, we see that the current best models are inadequate at precise point cloud completion. We discuss the reasons for this behavior - (1) We investigate synthetic and real-world world point clouds using tools from algebraic topology and topological data analysis in Section 4.1. Our findings, though striking are not surprising. The observation suggests that **RealPC** consists of non-trivial 0 and 1-dimensional Homology-based topological features that correspond to connected components, and cycles. This is indicated by the non-diagonal nature of the persistence diagram in Figure 1. These topological features add to the complexity of **RealPC** and provide strong evidence of the existence of higher dimensional topological features. We demonstrate through experiments that adding these Homology priors as constraints to an existing model can improve completion to some degree (Sec. 6). (2) Point cloud in **RealPC** are collected from several different sensors. **RealPC** utilizes four different sensors for collecting the point clouds. This is a realistic setting in the real world where different sources of the incomplete point clouds may use sensors with different intrinsic characteristics. Different point cloud samples in such a case may follow different distributions - which is not true in the synthetic datasets. (3) We demonstrate in Section 4.1 that real-world point clouds have several characteristics that make them challenging to work with compared to synthetic point clouds. These characteristics - (non-uniformity, noise, topological features) have a relatively uniform pattern in synthetic point clouds (Table 2). On the contrary, a real-world point cloud acquisition pipeline is affected by

several ungovernable parameters. These factors introduce non-uniform and inconsistent patterns that are challenging to model.

## 6 Persistent Homology Regularized Completion

We establish in Section 4.1 that **RealPC** consists of rich topological features while synthetic features lack these.

In this section, we focus on validating whether using topological priors on a suitable benchmarked work can improve the completion performance.

A challenge with using  $\mathcal{PH}$  is that it is compute-intensive. The computation of persistence and simplicies in the simplicial complex generated using the point clouds increases exponentially with the number of points. This makes it difficult to integrate with large-scale point cloud applications. We select a Point Cloud completion model that can be easily integrated with **PH**. We choose ODGNet [6] as our reference model to integrate  $\mathcal{PH}$ . We provide our reasons for selecting ODGNet as the reference model - ODGNet is an encoder-decoder network that works by predicting multi-scale features at the decoder. These are used to extract seed point clouds at different resolutions. ODGNet works by progressively up-scaling these at the decoder, and finally predicting the original point cloud. The sparse seed points clouds can be easily integrated with simple topological priors with moderate compute requirements. The availability of such point clouds as learnable parameters at intermediate layers in ODGNet also helps in training using the  $\mathcal{PH}$  based topological loss function.

### 6.1 Architecture

We describe the methodology for the integration of ODGNet with topological priors -**TOPODGnet**. We extract the multi-level seeds from the mid-level, low-level, and global features generated at the decoder. Seed points clouds consisting of points in the range of 256 to 1024 can be extracted at the decoder (Figure 6). The coarse nature of these seeds makes them easy to work with, as well as allows efficient computation of topological features.

#### 6.1.1 Topological Loss

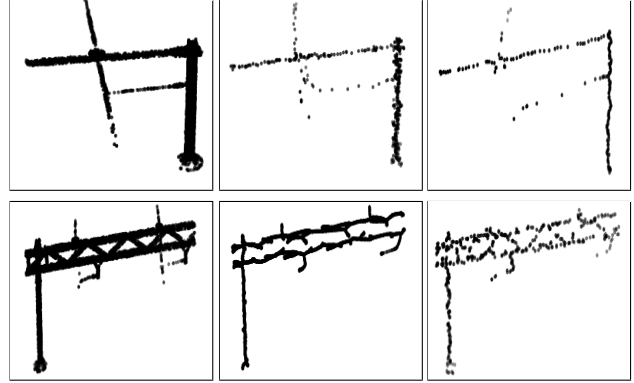


Figure 7: **Left:** A complete point cloud **Middle:** Visualization of the 0-dim  $\mathcal{PH}$  based skeleton on a sparse seed during initial training. **Right:** 0-dim  $\mathcal{PH}$  skeleton using sparse seeds as the training progresses. These priors assist the model in generating topologically consistent complete point clouds.

Given an incomplete point cloud, our goal is to augment new points that follow the global topology of the ground truth complete point cloud. We extract the coarse point cloud seeds at the decoder. Our aim is to ensure that the completed point cloud follows the global topology of the ground truth complete point cloud available in the dataset. Part of this work is already handled by the dictionary module of ODGNet[6]. It ensures that the seed point clouds are able to capture the artifacts of the complete point cloud.

We now apply topological regularization priors on the seed point clouds. To obtain this global topology-based backbone we use 0-dim  $\mathcal{PH}$  priors on the seed point clouds. 0-dim  $\mathcal{PH}$  ensures the extraction of a complete point cloud skeleton (Fig. 7) that can serve as a prior to the network to follow, for the complete point cloud generation. The underlying idea is to ensure the shape consistency of the complete output along the skeleton by generating points along the skeleton. We explain the process that extracts 0-dim  $\mathcal{PH}$  priors from the seeds - Given a seed point cloud we convert the seeds into a simplicial complex. The initial complex is just the original point clouds with  $\alpha$ -radius ball where  $\alpha=0$ . Increasing  $\alpha$  adds edges, faces to the simplicial complex, thereby leading to the evolution and death of  $k$ -dim topological features. Each  $k$ -dim topological feature is characterized by a  $(birth, death)$  pair.

Our goal is to use 0-dim  $\mathcal{PH}$  based topological features. These focus on the global topology of the point cloud, thereby providing a global skeleton that outlines the complete point cloud (Figure 7).

Each of the 0-dim homology features generated using filtration consists of a separate set of  $(birth, death)$  pairs de-

Baseline	RealPC Categories																					
	Ch0	Ch1	Ch2	Ch3	Du0	Du1	Du2	Du3	Du4	Hu0	Hu1	Hu2	Hu3	Hu4	Hu5	Hu6	Hu7	Sn0	Sn1	Sn2	Sn3	Mean
ODG	96	91	90	100	170	172	208	154	191	89	114	106	120	116	120	134	119	83	67	79	80	112
PoinTr	110	113	101	104	99	113	98	92	105	191	146	165	106	132	194	94	121	117	151	144	151	114
AdaPoinTr	65	71	71	68	57	54	52	98	37	158	132	114	75	79	134	67	86	65	47	61	53	69
FoldingNet	158	163	181	246	159	143	203	259	161	181	205	154	221	183	235	219	211	142	107	102	74	167
PCN	145	136	132	123	158	146	167	181	118	170	129	150	139	126	196	118	151	148	106	125	113	143
TopNet	563	385	200	211	88	77	90	91	45	590	110	328	94	79	441	93	93	455	75	320	129	341
SnowFlakenet	58	-	49	-	54	73	57	-	-	-	-	-	68	-	-	-	-	-	57	-	82	<b>60</b>
GRNet	79	80	79	104	83	63	66	111	64	140	133	131	92	74	155	74	82	81	71	94	73	84
Anchorformer	64	68	75	115	58	51	62	84	36	146	131	108	79	85	151	70	92	78	79	75	91	87

Table 2: Benchmark results on the **RealPC**. Despite remarkable performance on synthetic datasets, the baselines fail on **RealPC**

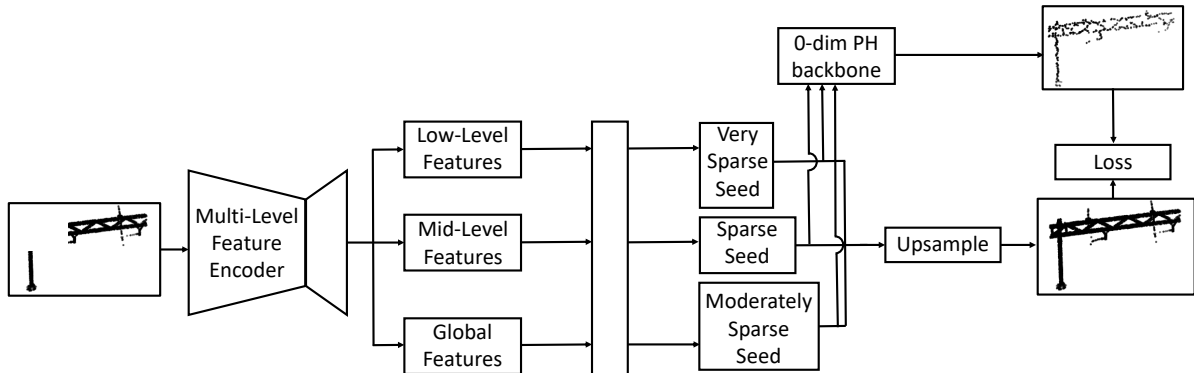


Figure 6: Architecture diagram of **TOPODGnet**. We calculate  $0\text{-dim } \mathcal{PH}$  based topological priors over the sparse seeds and integrate it into the loss function. It enables completion along a topologically consistent skeleton.

noted as  $b, d$ . The persistence of each pair is  $(b-d)$ .

Now we explain our topological loss function - For  $0\text{-dim } \mathcal{PH}$ , we minimize the sum of persistence values for the pairs. This ensures that at the end of the filtration, there is one connected component left (given that we minimize the persistence of all the pairs *and* there always exists at least 1 component by default in the persistence diagram). This persistence diagram outlines the skeleton of the complete point cloud, which when used as a regularizer to a model, guides point generation along the skeleton. Given  $(b_i, d_i)$  are the  $(\text{birth}, \text{death})$  pairs of a given seed point cloud, the topology loss  $L_{\text{homo}}$  is defined as follows -

$$\mathcal{L}_{\text{homo}} = \sum_{i=0}^n 1_{\{i > k\}}(b_i - d_i) = \sum_{i=k+1}^n (b_i - d_i) \quad (1)$$

We explain the significance of  $k$  now. The input partial point cloud may not necessarily have a single component- but may be split into more than one component (Fig. 6). In

such cases, using  $k \geq 2$ , allows  $\mathcal{PH}$  to generate multiple skeletons - each of which can attend to partial components in the input.

## 6.2 Results

Method	CD-L1	CD-L2
ODGNet	112.6	87.3
ODGNet with $0\text{-dim } \mathcal{PH}$	<b>103.6</b>	<b>80.1</b>

Table 3: Performance of ODGNet with and without topology regularization.

We demonstrate the effect of topology on the ODGNet backbone. Figure 8 shows the topologically consistent output of **TOPODGnet** relative to the baseline - which in turn results in a reduced Chamfer distance in Table 3. While both the outputs are still noisy, **TOPODGnet**(middle) maintains a better topology when matched with the ground truth.

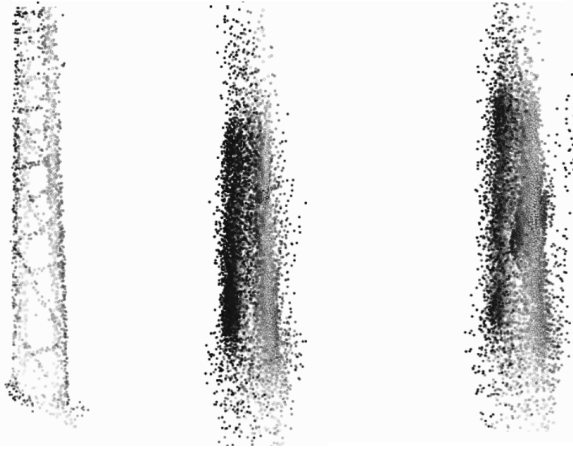


Figure 8: **Left:** Corresponding Ground Truth of a partial input to **TOPODGnet**. **Middle:** Output generated by **TOPODGnet**. **Right:** Output generated by ODGNet. We find that **TOPODGnet** is able to follow the global topology of the ground truth point cloud better than ODGNet(right), as indicated by the tapering upper half of the output and overall consistency. **TOPODGnet** shows visible benefits of introducing topological priors.

## 7 Conclusion

Real-world point clouds have several inherent characteristics that contrast them from synthetic point clouds - non-uniform density, noise, and presence of topological features. Current state-of-the-art methods for point cloud completion do not account for these, thereby failing miserably for real-world point clouds. We introduce the first *real world paired point cloud completion dataset- RealPC*. It consists of 21 categories across  $\sim 40,000$  pairs. We benchmark several state-of-the-art baselines on **RealPC** and demonstrate the need to rethink point cloud completion for the real world. We also demonstrate that utilizing Homology-based topological features of real-world point clouds as regularizers can help generate topologically accurate complete point clouds.

## References

- [1] SNCF Réseau railway dataset. <https://ressources.data.sncf.com/explore/dataset/nuage-points-3d/table/>, 2017. 4, 5
- [2] A. Alliegro, D. Valsesia, G. Fracastoro, E. Magli, and T. Tommasi. Denoise and contrast for category agnostic shape completion. In *CVPR*, 2021. 3
- [3] G. Bingchen, N. Yinyu, L. Yiqun, H. Xiaoguang, and Y. Yizhou. Me-pcn: Point completion conditioned on mask emptiness. In *ICCV*, 2021. 3
- [4] R. Brüel-Gabrielsson, V. Ganapathi-Subramanian, P. Skraba, and L. J. Guibas. Topology-aware surface reconstruction for point clouds. In *Computer Graphics Forum*, volume 39, pages 197–207. Wiley Online Library, 2020. 3
- [5] R. Brüel-Gabrielsson, V. Ganapathi-Subramanian, P. Skraba, and L. Guibas. Topology-aware surface reconstruction for point clouds. *arXiv preprint arXiv:1811.12543*, 2019. 3
- [6] P. Cai, D. Scott, X. Li, and S. Wang. Orthogonal dictionary guided shape completion network for point cloud. In *AAAI*, 2024. 3, 5, 7, 2
- [7] R. J. Campello, D. Moulavi, and J. Sander. Density-based clustering based on hierarchical density estimates. In *Pacific-Asia conference on knowledge discovery and data mining*, pages 160–172. Springer, 2013. 4
- [8] Z. Cang, L. Mu, and G.-W. Wei. Representability of algebraic topology for biomolecules in machine learning based scoring and virtual screening. *PLoS computational biology*, 14(1):e1005929, 2018. 2
- [9] G. Carlsson, A. Zomorodian, A. Collins, and L. Guibas. Persistence barcodes for shapes. In *Proceedings of the 2004 Eurographics/ACM SIGGRAPH symposium on Geometry processing*, pages 124–135, 2004. 3
- [10] A. Chang, A. Dai, T. Funkhouser, M. Halber, M. Niessner, M. Savva, S. Song, A. Zeng, and Y. Zhang. Matterport3d: Learning from rgb-d data in indoor environments. *arXiv preprint arXiv:1709.06158*, 2017. 2
- [11] A. X. Chang, T. Funkhouser, L. Guibas, P. Hanrahan, Q. Huang, Z. Li, S. Savarese, M. Savva, S. Song, H. Su, et al. Shapenet: An information-rich 3d model repository. *arXiv preprint arXiv:1512.03012*, 2015. 2
- [12] C. Chen, X. Ni, Q. Bai, and Y. Wang. A topological regularizer for classifiers via persistent homology. In *The 22nd International Conference on Artificial Intelligence and Statistics*, pages 2573–2582. PMLR, 2019. 3
- [13] Z. Chen, F. Long, Z. Qiu, T. Yao, W. Zhou, J. Luo, and T. Mei. Anchorformer: Point cloud completion from discriminative nodes. In *Proceedings of the IEEE/CVF conference on computer vision and pattern recognition*, pages 13581–13590, 2023. 2
- [14] J. R. Clough, I. Oksuz, N. Byrne, J. A. Schnabel, and A. P. King. Explicit topological priors for deep-learning based image segmentation using persistent homology. In *International Conference on Information Processing in Medical Imaging*, pages 16–28. Springer, 2019. 3
- [15] M. Cserep. Hungarian mls point clouds of railroad environment and annotated ground truth data. *Mendeley Data*. DOI: <https://doi.org/10.17632/ccxpzhx9dj>, 1, 2022. 4, 5
- [16] R. Cui, S. Qiu, S. Anwar, J. Liu, C. Xing, J. Zhang, and N. Barnes. P2c: Self-supervised point cloud completion from single partial clouds. In *Proceedings of the IEEE/CVF International Conference on Computer Vision*, pages 14351–14360, 2023. 5

- [17] A. Dai, A. X. Chang, M. Savva, M. Halber, T. Funkhouser, and M. Nießner. Scannet: Richly-annotated 3d reconstructions of indoor scenes. In *Proceedings of the IEEE conference on computer vision and pattern recognition*, pages 5828–5839, 2017. 2
- [18] T. K. Dey, K. Li, C. Luo, P. Ranjan, I. Safa, and Y. Wang. Persistent heat signature for pose-oblivious matching of incomplete models. In *Computer Graphics Forum*, volume 29, pages 1545–1554. Wiley Online Library, 2010. 3
- [19] H. Edelsbrunner. Computational topology an introduction, 2008. 1
- [20] H. Edelsbrunner and J. Harer. *Computational Topology - an Introduction*. American Mathematical Society, 2010. 3
- [21] B. Fei, W. Yang, W.-M. Chen, Z. Li, Y. Li, T. Ma, X. Hu, and L. Ma. Comprehensive review of deep learning-based 3d point cloud completion processing and analysis. *IEEE Transactions on Intelligent Transportation Systems*, 23(12):22862–22883, 2022. 2
- [22] R. B. Gabrielsson and G. Carlsson. Exposition and interpretation of the topology of neural networks. In *2019 18th IEEE international conference on machine learning and applications (icmla)*, pages 1069–1076. IEEE, 2019. 3
- [23] R. B. Gabrielsson, B. J. Nelson, A. Dwaraknath, and P. Skraba. A topology layer for machine learning. In *International Conference on Artificial Intelligence and Statistics*, pages 1553–1563. PMLR, 2020. 3
- [24] T. Gebhart and P. Schrater. Adversarial examples target topological holes in deep networks. *arXiv preprint arXiv:1901.09496*, 2019. 3
- [25] A. Geiger, P. Lenz, and R. Urtasun. Are we ready for autonomous driving? the kitti vision benchmark suite. In *2012 IEEE Conference on Computer Vision and Pattern Recognition*, pages 3354–3361. IEEE, 2012. 2
- [26] H. Geng, Z. Li, Y. Geng, J. Chen, H. Dong, and H. Wang. Partmanip: Learning cross-category generalizable part manipulation policy from point cloud observations. In *Proceedings of the IEEE/CVF Conference on Computer Vision and Pattern Recognition*, pages 2978–2988, 2023. 2
- [27] N. Giansiracusa, R. Giansiracusa, and C. Moon. Persistent homology machine learning for fingerprint classification. *arXiv preprint arXiv:1711.09158*, 2017. 3
- [28] Z. Guo, H. Liu, H. Shi, F. Li, X. Guo, and B. Cheng. Kd-tree-based euclidean clustering for tomographic sar point cloud extraction and segmentation. *IEEE Geoscience and Remote Sensing Letters*, 20:1–5, 2023. 2
- [29] C. Hofer, R. Kwitt, M. Niethammer, and A. Uhl. Deep learning with topological signatures. *Advances in neural information processing systems*, 30, 2017. 3
- [30] T. Hu, Z. Han, and M. Zwicker. 3d shape completion with multi-view consistent inference. In *AAAI*, 2020. 3
- [31] S. Li, P. Gao, X. Tan, and M. Wei. Proxyformer: Proxy alignment assisted point cloud completion with missing part sensitive transformer. In *Proceedings of the IEEE/CVF conference on computer vision and pattern recognition*, pages 9466–9475, 2023. 2
- [32] J.-Y. Liu, S.-K. Jeng, and Y.-H. Yang. Applying topological persistence in convolutional neural network for music audio signals. *arXiv preprint arXiv:1608.07373*, 2016. 3
- [33] M. Moor, M. Horn, B. Rieck, and K. Borgwardt. Topological autoencoders. In *International conference on machine learning*, pages 7045–7054. PMLR, 2020. 3, 2
- [34] M. Nguyen, M. Aktas, and E. Akbas. Bot detection on social networks using persistent homology. *Mathematical and Computational Applications*, 25(3):58, 2020. 2
- [35] M. Nguyen, S. Vats, S. Van Damme, J. Van Der Hooft, M. T. Vega, T. Wauters, C. Timmerer, and H. Hellwagner. Impact of quality and distance on the perception of point clouds in mixed reality. In *2023 15th International Conference on Quality of Multimedia Experience (QoMEX)*, pages 87–90. IEEE, 2023. 2
- [36] L. Pan, X. Chen, Z. Cai, J. Zhang, H. Zhao, S. Yi, and Z. Liu. Variational relational point completion network. In *Proceedings of the IEEE/CVF conference on computer vision and pattern recognition*, pages 8524–8533, 2021. 2
- [37] L. Pan, X. Chen, Z. Cai, J. Zhang, H. Zhao, S. Yi, and Z. Liu. Variational relational point completion network. In *CVPR*, 2021. 3
- [38] A. Poulenard, P. Skraba, and M. Ovsjanikov. Topological function optimization for continuous shape matching. In *Computer Graphics Forum*, volume 37, pages 13–25. Wiley Online Library, 2018. 3
- [39] C. S. Pun, K. Xia, and S. X. Lee. Persistent-homology-based machine learning and its applications—a survey. *arXiv preprint arXiv:1811.00252*, 2018. 3
- [40] B. Qiu, Y. Zhou, L. Dai, B. Wang, J. Li, Z. Dong, C. Wen, Z. Ma, and B. Yang. Whu-railway3d: A diverse dataset and benchmark for railway point cloud semantic segmentation. *IEEE Transactions on Intelligent Transportation Systems*, 2024. 4, 5
- [41] M. Sarmad, H. J. Lee, and Y. M. Kim. RI-gan-net: A reinforcement learning agent controlled gan network for real-time point cloud shape completion. In *CVPR*, 2019. 3
- [42] Y. Singh, C. M. Farrelly, Q. A. Hathaway, T. Leiner, J. Jagtap, G. E. Carlsson, and B. J. Erickson. Topological data analysis in medical imaging: current state of the art. *Insights into Imaging*, 14(1):1–10, 2023. 2
- [43] L. P. Tchapmi, V. Kosaraju, H. Rezatofighi, I. Reid, and S. Savarese. Topnet: Structural point cloud decoder. In *Proceedings of the IEEE/CVF conference on computer vision and pattern recognition*, pages 383–392, 2019. 2
- [44] L. P. Tchapmi, V. Kosaraju, H. Rezatofighi, I. Reid, and S. Savarese. Topnet: Structural point cloud decoder. In *CVPR*, 2019. 3, 5
- [45] K. W. Tesema, L. Hill, M. W. Jones, M. I. Ahmad, and G. K. Tam. Point cloud completion: A survey. *IEEE Transactions on Visualization and Computer Graphics*, 2023. 2
- [46] H. Tianxin, Z. Hao, C. Jinhao, Y. Xuemeng, W. Mengmeng, Z. Xiangrui, Z. Jiangning, Y. Yi, X. Yifan, and L. Yong. Rfnet: Recurrent forward network for dense point cloud completion. In *ICCV*, 2021. 3

- [47] B. Ton. Labelled high resolution point cloud dataset of 15 catenary arches in the netherlands. *4TU Res. data, The NetherlandsTech. Rep.*, 2022. 4, 5
- [48] J. Wang, Y. Cui, D. Guo, J. Li, Q. Liu, and C. Shen. Pointattn: You only need attention for point cloud completion. In *Proceedings of the AAAI Conference on artificial intelligence*, volume 38, pages 5472–5480, 2024. 2
- [49] J. Wang, Y. Cui, D. Guo, J. Li, Q. Liu, and C. Shen. Pointattn: You only need attention for point cloud completion. *Proceedings of the AAAI Conference on Artificial Intelligence*, 38(6):5472–5480, Mar. 2024. 3, 5
- [50] X. Wen, P. Xiang, Z. Han, Y.-P. Cao, P. Wan, W. Zheng, and Y.-S. Liu. Pmp-net: Point cloud completion by learning multi-step point moving paths. In *CVPR*, 2021. 3
- [51] T. Wu, J. Zhang, X. Fu, Y. Wang, J. Ren, L. Pan, W. Wu, L. Yang, J. Wang, C. Qian, et al. Omniobject3d: Large-vocabulary 3d object dataset for realistic perception, reconstruction and generation. In *Proceedings of the IEEE/CVF Conference on Computer Vision and Pattern Recognition*, pages 803–814, 2023. 2
- [52] P. Xiang, X. Wen, Y.-S. Liu, Y.-P. Cao, P. Wan, W. Zheng, and Z. Han. Snowflakenet: Point cloud completion by snowflake point deconvolution with skip-transformer. In *Proceedings of the IEEE/CVF international conference on computer vision*, pages 5499–5509, 2021. 2, 3, 5
- [53] P. Xiang, X. Wen, Y.-S. Liu, Y.-P. Cao, P. Wan, W. Zheng, and Z. Han. Snowflakenet: Point cloud completion by snowflake point deconvolution with skip-transformer. In *ICCV*, 2021. 3
- [54] H. Xie, H. Yao, S. Zhou, J. Mao, S. Zhang, and W. Sun. Grnet: Gridding residual network for dense point cloud completion. In *European conference on computer vision*, pages 365–381. Springer, 2020. 3, 6
- [55] Z. Xuancheng, F. Yutong, L. Siqi, Z. Changqing, W. Hai, Z. Xibin, G. Yandong, and G. Yue. View-guided point cloud completion. In *CVPR*, 2021. 3
- [56] X. Yu, Y. Rao, Z. Wang, Z. Liu, J. Lu, and J. Zhou. Pointr: Diverse point cloud completion with geometry-aware transformers. In *Proceedings of the IEEE/CVF international conference on computer vision*, pages 12498–12507, 2021. 2
- [57] X. Yu, Y. Rao, Z. Wang, Z. Liu, J. Lu, and J. Zhou. Pointr: Diverse point cloud completion with geometry-aware transformers. In *ICCV*, 2021. 3, 5
- [58] J. Yuan, B. Zhang, X. Yan, B. Shi, T. Chen, Y. Li, and Y. Qiao. Ad-pt: Autonomous driving pre-training with large-scale point cloud dataset. *Advances in Neural Information Processing Systems*, 36, 2024. 2
- [59] W. Yuan, T. Khot, D. Held, C. Mertz, and M. Hebert. Pcn: Point completion network. In *2018 international conference on 3D vision (3DV)*, pages 728–737. IEEE, 2018. 2, 3
- [60] W. Yuan, T. Khot, D. Held, C. Mertz, and M. Hebert. Pcn: point completion network. In *3DV*, 2018. 3
- [61] S. Zhang, X. Liu, H. Xie, L. Nie, H. Zhou, D. Tao, and X. Li. Learning geometric transformation for point cloud completion. *International Journal of Computer Vision*, pages 1–21, 2023. 2
- [62] R. Zhao, H. Wang, C. Zhang, and W. Cai. Pointneuron: 3d neuron reconstruction via geometry and topology learning of point clouds. In *Proceedings of the IEEE/CVF Winter Conference on Applications of Computer Vision*, pages 5787–5797, 2023. 2
- [63] H. Zhou, Y. Cao, W. Chu, J. Zhu, T. Lu, Y. Tai, and C. Wang. Seedformer: Patch seeds based point cloud completion with upsamle transformer. In *European conference on computer vision*, pages 416–432. Springer, 2022. 2, 3, 6
- [64] Z. Zhuang, Z. Zhi, T. Han, Y. Chen, J. Chen, C. Wang, M. Cheng, X. Zhang, N. Qin, and L. Ma. A survey of point cloud completion. *IEEE Journal of Selected Topics in Applied Earth Observations and Remote Sensing*, 2024. 2

# Revisiting Point Cloud Completion: Are We Ready For The Real-World?

## Supplementary Material

### 8 Persistent Homology

In this section, we delve into the concept of Persistent Homology ( $\mathcal{PH}$ ), an important tool in topological data analysis that systematically uncovers and quantifies the topological features of datasets. Persistent Homology combines ideas from algebraic topology, geometry, and computational mathematics to identify meaningful structures, such as connected components, loops, and voids, that persist across multiple scales. It is particularly valuable when applied to data in the form of point clouds or pixelated images, where traditional methods might struggle to capture structural and relational information.

At the core of this process lies the representation of a topological space as a cell complex—a combinatorial structure that encodes the relationships between points in the space. These cell complexes are constructed using simplices, which are the building blocks of higher-dimensional shapes. A 0-dimensional simplex is a point, a 1-dimensional simplex is an edge, a 2-dimensional simplex is a triangle, and so on, with higher-dimensional simplices being generalizations of these structures. Simplices are combined to form simplicial complexes, which generalize graphs to higher dimensions. Figure 9 provides a visual depiction of simplices of various dimensions and how they combine to form simplicial complexes. These structures serve as the foundation for applying homological methods.

Homology, in its simplest sense, is a branch of mathematics that provides a systematic way to analyze and classify the global properties of a topological space by examining its local features. Specifically, homology assigns algebraic invariants to a topological space, allowing us to identify and quantify  $k$ -dimensional holes, where  $k$  corresponds to the dimension of the feature being analyzed. For example: a 0-dimensional hole corresponds to a connected component of the space, a 1-dimensional hole corresponds to a loop or cycle, a 2-dimensional hole corresponds to a void or cavity enclosed by a surface.

These holes, generalized across all dimensions, encapsulate the structural essence of a space. Figure 9 illustrate how homology captures these features, translating the geometry of a space into meaningful topological features [19].

Persistent Homology ( $\mathcal{PH}$ ) extends classical homology by tracking how these  $k$ -dimensional features change as the dataset is viewed at different scales. This is accomplished by constructing a filtration, which is a sequence of nested simplicial complexes:

$$\phi \subseteq \mathcal{C}_1 \subseteq \mathcal{C}_2 \subseteq \mathcal{C}_3 \dots \mathcal{C}_i \dots \mathcal{C}_n = \mathcal{C},$$

where  $\phi$  is the empty complex, and  $\mathcal{C}$  is the final simplicial complex encompassing the entire dataset. Each step in this sequence corresponds to a specific scale or resolution. Persistent Homology identifies when topological features, such as connected components, cycles, or voids, are born and when they die as the filtration progresses. Features that persist across a wide range of scales are considered significant and indicative of meaningful structures within the data. Conversely, features that appear and disappear quickly are often interpreted as noise [19].

Filtration is the step-by-step process of building simplicial complexes by progressively adding simplices to the structure. The manner in which this process is defined depends on the type of dataset being analyzed. For example, in the case of point clouds, a filtration is often constructed using distances between points. At each stage of the filtration, new simplices are added based on a chosen threshold parameter, often denoted by  $\alpha$ . The filtration progresses monotonically, meaning that each simplicial complex in the sequence contains all simplices from the previous step, along with any new simplices added at that stage.

For point clouds, a common type of filtration is the Vietoris–Rips filtration, which is defined based on pairwise distances between points. For a given value of  $\alpha$ , an edge is added between two points if the distance between them is less than or equal to  $2\alpha$ . Higher-dimensional simplices, such as triangles and tetrahedra, are introduced when a set of points becomes fully connected. The progression of this filtration is depicted in Table 9, which illustrates how simplicial complexes evolve as  $\alpha$  increases.

As the filtration progresses, topological features are born and die. These events are recorded as pairs  $(b, d)$ , where  $b$  is the scale at which the feature first appears (birth), and  $d$  is the scale at which the feature disappears (death). For example: - The addition of an edge may create a new 1-dimensional cycle, marking the birth of a feature. - Conversely, the addition of another edge may fill in that cycle, causing its death.

Consider the example of four points forming a rectangle. Initially, a 1-dimensional hole (cycle) is created when the rectangle is formed. When the diagonal edge is added, the rectangle is divided into two triangles (2-simplices), resulting in the destruction of the cycle. These birth-death pairs can be visualized using barcodes, where the length of each bar represents the persistence of a feature. Long bars correspond to significant features, while short bars typically represent noise [19].

When dealing with images, the process of constructing a filtration differs from that of point clouds. Instead of us-

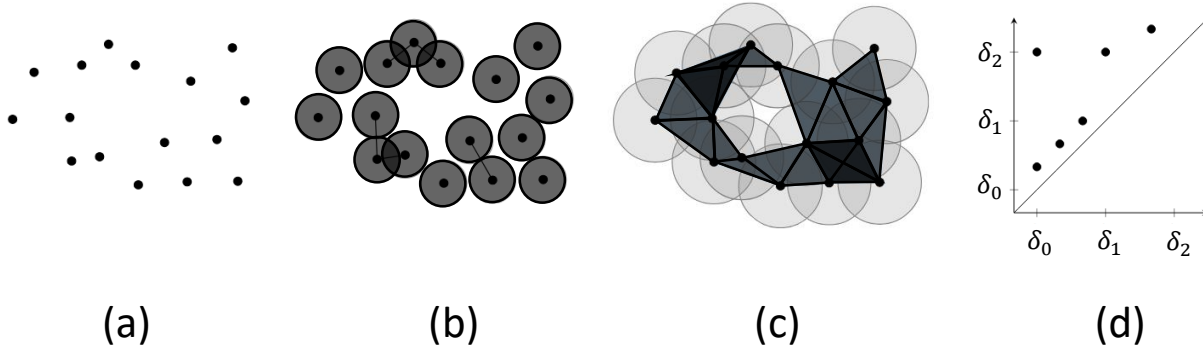


Figure 9: Left to Right (a to c). Progression of filtration on a point cloud over different spatial resolutions as the distance threshold increases [33]. Creation and destruction of  $k - dim$  topological features documented in (d) which is a persistence diagram representing  $(b_i, d_i)$  pairs - each point corresponds to a  $k - dim$  homology that takes birth at  $b_i$  and dies at  $d_i$ .

ing pairwise distances, the pixel intensities of the image are used. The final simplicial complex  $\mathcal{C}$  corresponds to a triangulation of the image grid, with vertices representing pixels. Sub-level set filtrations are used, where the filtration function is defined as:

$$f((v_0, v_1 \dots v_n)) = \max_{i=0,1,2,3 \dots n} f(v_i),$$

which assigns each simplex a value equal to the maximum intensity of its vertices. Filtration begins with the minimum intensity value and gradually includes pixels with intensities less than or equal to  $\alpha$ . As  $\alpha$  increases, new simplices are added, and the filtration progresses. This allows the topological features of the image to be analyzed at multiple intensity levels.

Persistent Homology is a powerful framework that extracts meaningful structural information from complex datasets. By studying the persistence of topological features across scales, it provides insights into the underlying geometry and topology of the data. Its versatility makes it applicable to a wide range of domains, including shape analysis, image processing, and network analysis.

## 9 Topological Loss Function

The topological loss function assists the completion process by ensuring that the model generates point clouds along the topological prior generated by  $0-dim \mathcal{PH}$ .

The coarse point cloud seeds at the decoder assist the topological module and are used as input for the topological loss. The output of the topological module consists of  $0-dim$  topological features (*birth, death*) pairs. The loss function in Equation 2 uses these pairs for adjusting the *birth* and *death* values of the  $0-dim$  Homology features according to the required skeleton and the available components in the input incomplete point cloud.

$$\mathcal{L}_{homo} = - \sum_{i=0}^n 1\{i > k\} (b_i - d_i) = - \sum_{i=k+1}^n (b_i - d_i) \quad (2)$$

The parameter  $k$  holds significance here. As explained in the main paper, the input partial point cloud may consist of multiple disconnected components as demonstrated in Figure Figure 6 in the main paper. In such cases, the above loss formulation ensures that the skeleton can have three skeleton components that can (a) cater to the three disconnected components and (b) merge together to form the final complete point cloud skeleton.

Setting the value of  $k$  requires manual inspection of the partial complete point clouds. In cases where the majority of points clouds have single components, setting  $k=l$  works fairly well.

This formulation assists in the formation of the  $0-dim \mathcal{PH}$  skeleton easily when the partial point clouds are not continuous (points are in disconnected cluster).

## 10 Experimental Details

We provide the experimental details here. Our models are trained using an NVIDIA A100 GPU. For training the **TOPODGnet** we use the same parameters and model structure as ODGNet [6]. We plug in the topology module on the sparse seeds generated at the decoder as demonstrated in Figure 6 in the main paper.

## 11 Demonstrations

We visually demonstrate nine point clouds from our dataset in Table 4 and 5. These demonstrate the non-uniform sparsity and noise that are natural and intrinsic characteristics of real-world datasets. We demonstrate the

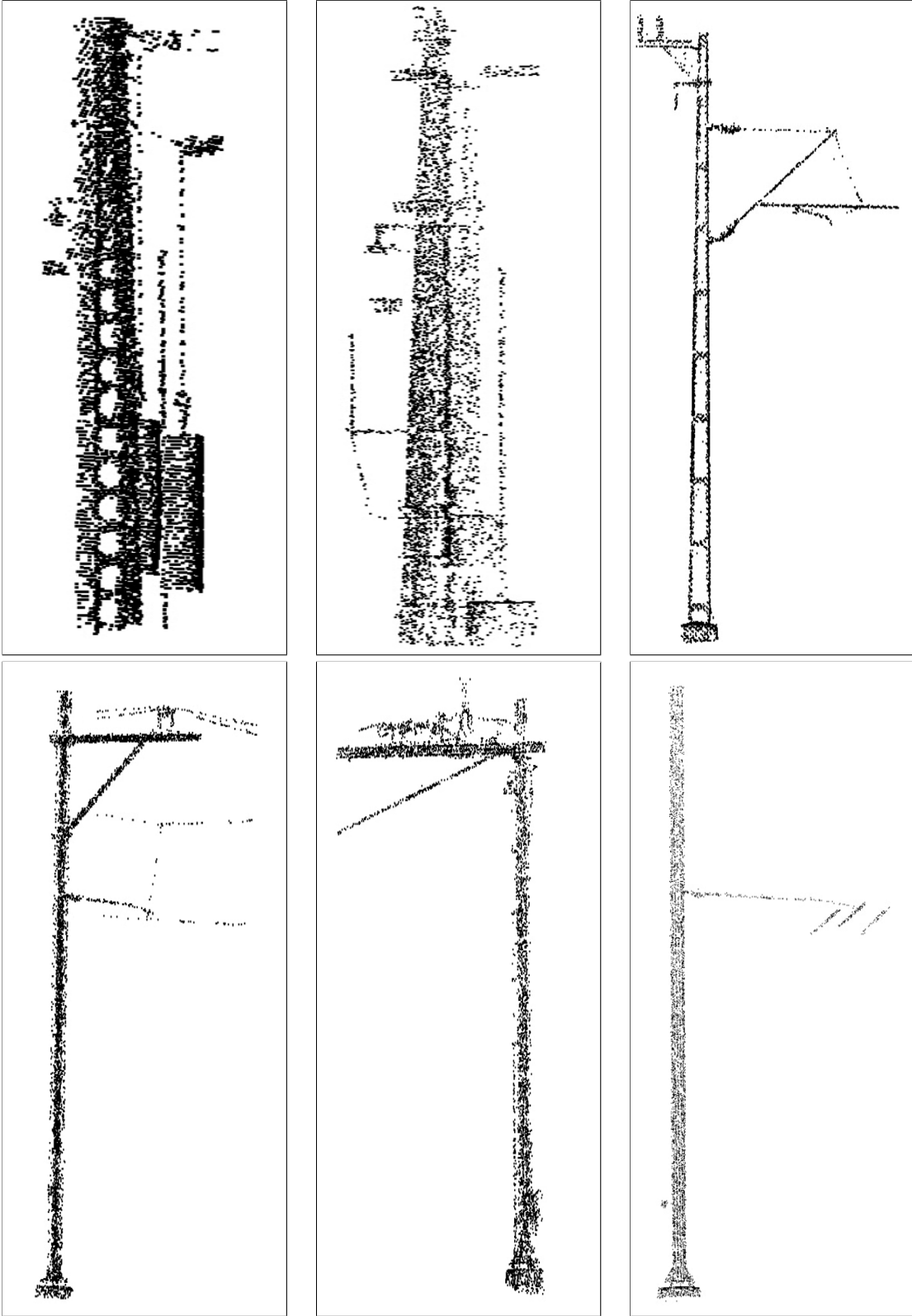


Table 4: Visual Demonstration of some examples from our dataset. For a video demonstration please refer to the video in the supplementary.

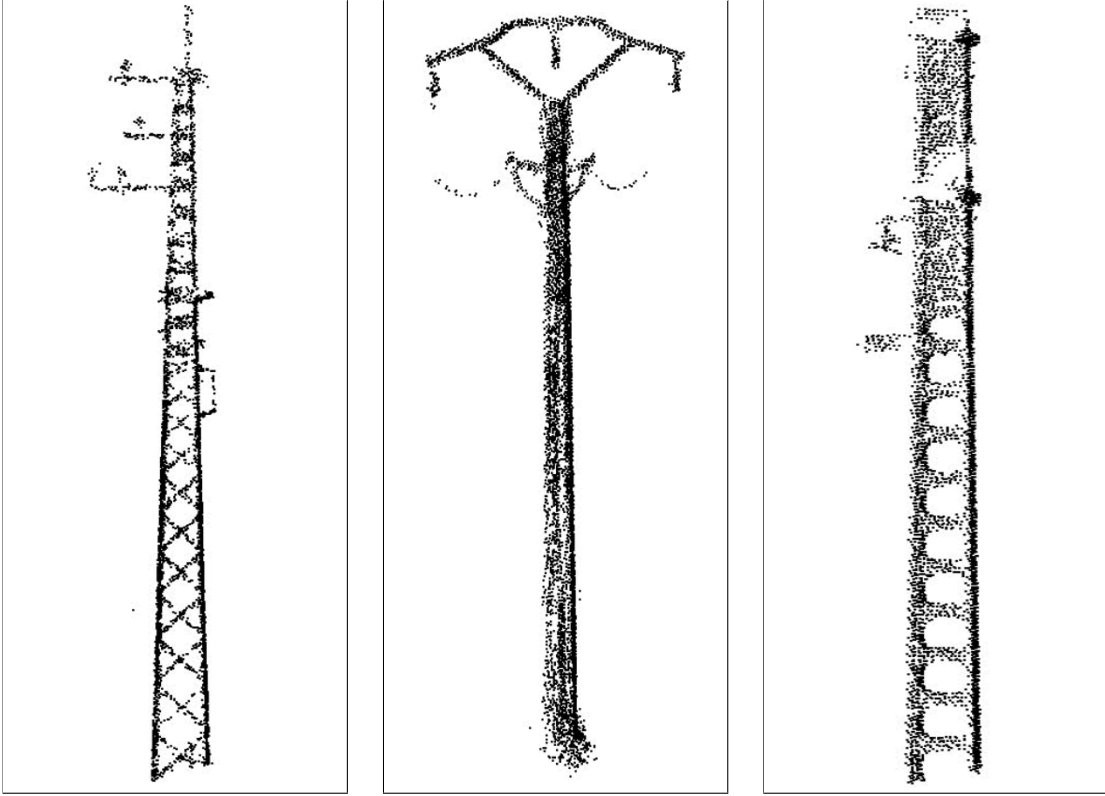


Table 5: Visual Demonstration of some examples from our dataset. For a video demonstration please refer to the video in the supplementary.

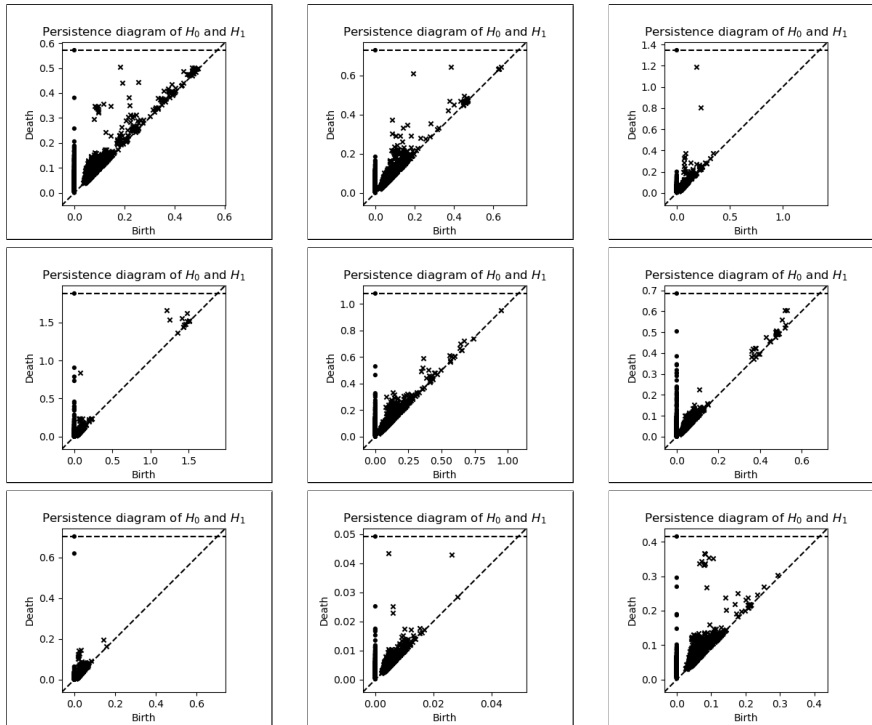


Table 6: Persistence Diagram of nine point clouds (of Table 4 and 5) of the **RealPC** dataset.

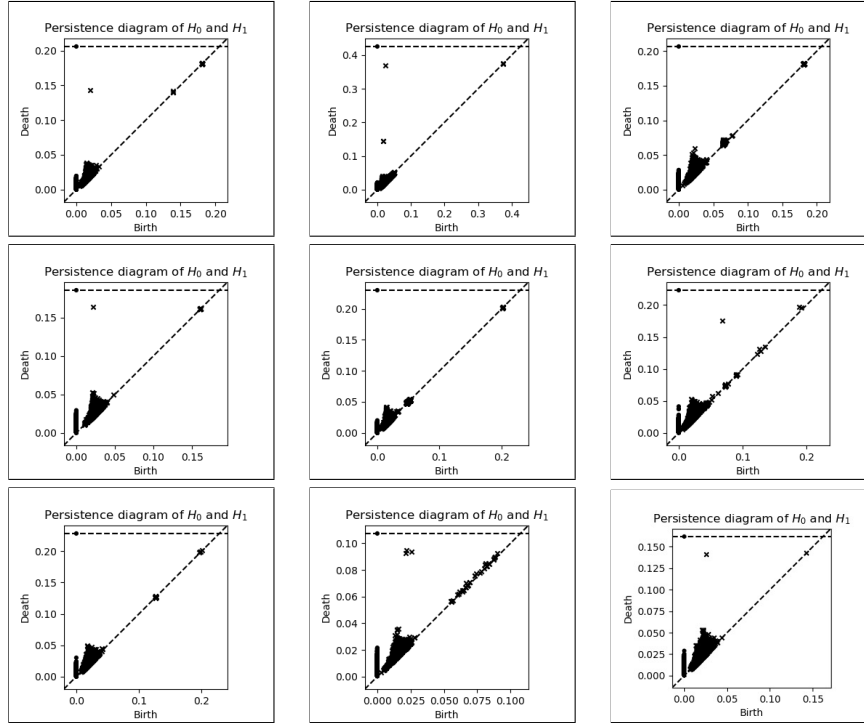


Table 7: Persistence Diagram of nine point clouds from the synthetic datasets - ShapeNet and PCN.

Persistence Diagrams of these nine point clouds in Figure 6. For most of the point clouds we observe non-trivial persistence (most points are far from the diagonal). This indicates that real-world point clouds captured in challenging settings exhibit significant zero and one-dimensional topological features which are absent in synthetic point clouds (refer to Table 1 in the main paper). These persistence features are not observed in the persistence diagram of the synthetic datasets as shown in Table 7. Almost all the 0-dimensional topological features (indicated by dot) are along or very close to the diagonal for the synthetic datasets (Table 7) as opposed to **RealPC** (Table 6).